Multi-periodic repetitive control for functional electrical stimulation based wrist tremor suppression

Zan Zhang, Bing Chu, Yanhong Liu, Haichuan Ren, Zhe Li and David H Owens

***Abstract*— Intention tremor refers to the rhythmic and involuntary contraction and relaxation of muscles with movement towards a target, which is a common sequela of multiple sclerosis and usually occurs in the distal joints of the upper limb. Functional electrical stimulation (FES) is feasible for tremor suppression because of its fewer side effects, low-cost and portability. Most existing FES based design methods assume that tremor is a single frequency signal, though it is multi-frequency in reality. The idealized simplification will limit the performance of tremor suppression. To address the problem, this paper proposes an FES-based multi-periodic repetitive control scheme to suppress multiple frequency wrist tremor. Firstly, a nonlinear wrist musculoskeletal model with Hammerstein structure is established. Then, a control strategy combining the model inverse linearization control and multi-periodic repetitive control is proposed for tremor suppression. A frequency modified inverse repetitive control algorithm and a gradient-based repetitive control algorithm are developed to regulate the FES level. Finally, comparative experiments on four unimpaired participants and an intention tremor patient are conducted to validate the effectiveness of the proposed control schemes. Experimental results show that the multi-periodic repetitive control scheme can suppress tremor by up to 90.52%. Compared with the traditional filter based feedback controller and the single periodic repetitive controller, the proposed multi-periodic repetitive controller can achieve an average of 26% and 16% improvement respectively in tremor suppression, demonstrating the advantages of the proposed design.**

***Index Terms*— Wrist tremor suppression, functional electrical stimulation (FES), multi-periodic repetitive control, simulation and experimental verification.**

I. Introduction

Zan Zhang, Yanhong Liu, Haichuan Ren and David H Owens are with School of Electrical Engineering, Zhengzhou University, Zhengzhou, China, (e-mail: zanzan@zzu.edu.cn, liuyh@zzu.edu.cn, rhc@zzu.edu.cn).

Bing Chu is with Department of Electronics and Computer Science, University of Southampton, Southampton, SO17 1BJ, UK (e-mail: B.Chu@soton.ac.uk).

Zhe Li is with the Rehabilitation Department, Fifth Affiliated Hospital of Zhengzhou University, Zhengzhou, China (e-mail: lizhe.1974@163.com).

David H Owens is also with Department of Automatic Control and Systems Engineering, The University of Sheffield, Mappin Street, Sheffield, S1 3JD, UK (e-mail:d.h.owens@sheffield.ac.uk).

This work is supported by the National Key Research and Development Project (No. 2020YFB1313701), the National Natural Science Foundation of China (No. 61803344, 62003309) and the Outstanding Foreign Scientist Support Project in Henan Province (No. GZS2019008).

Corresponding author: Yanhong Liu

MULTIPLE sclerosis is an inflammatory and degenerative disease of the central nervous system and is one of the most diagnosed neurological disorders [1]. A common symptom of multiple sclerosis is intention tremor, which usually occurs when the upper limb of patients is about to reach a certain target. This kind of involuntary and oscillating movement causes great difficulties and embarrassments to patients' daily activities (although it is not life threatening) [2]. Therefore, how to carry out rehabilitation training for patients to effectively suppress tremor has become an important research subject. Though there are a variety of treatment options for tremor patients, they all have some limitations: long term use of prescription medication may result in serious side effects and drug tolerance [3]; neurosurgical operations, such as stereotactic thalamotomy [4], stereotactic pallidotomy [5] and deep brain stimulation [6] require the invasive brain surgery – the cost of surgery is high and there is a risk of postoperative complications [7]; mechanical systems such as exoskeleton robots are bulky and inconvenient for patients' daily rehabilitation [8].

Functional electrical stimulation (FES) provides an alternative [9]–[11] and has attracted wide interests due to its minor side effects, low-cost and highly portability [12]–[15]. Moreover, FES is a kind of artificial electrical stimulation, which can directly activate motor neurons to make muscles contract and achieve the purpose of motor function recovery and reconstruction [16].

The FES based tremor suppression system aims to generate anti-phase electrical pulse with respect to tremor movement, promote muscle contraction and reduce tremor amplitude. This FES technique is generally applied in a closed-loop feedback control system to adjust the timing and level of FES applied to muscles to suppress tremor. The filter based controller was first developed in [12], [17] and the suppression performance of wrist and elbow joint tremor was tested by three different types of patients: the amplitude attenuation of 75% at 3.4Hz of essential tremor, 81% at 3.4Hz of Parkinsonian tremor and 60% at 2.1Hz of cerebellar tremor were achieved respectively. In [18], a controller based on digital filter was used to suppress tremor and the performance was better than that based on analog filter. The average tremor attenuation for the no neurological impairment subjects was 68.9% for the analog system and 83.1% for the digital system at 4Hz. A controller combining fuzzy logic control and proportional derivative control was developed in [19] for tremor suppression. Simulation

results showed that the tremor level of 8Hz can be significantly reduced by about 85%. Zhang et al used a neural oscillator based FES to suppress tremor and a PID controller to regulate the stimulation level of FES [14]. Tremor attenuation of 90% was achieved on average at certain single frequency, but the control performance was not verified by experiments. Because tremor is mainly manifested in rhythmic and periodic motion [2], repetitive control (RC) is very suitable for suppressing tremor. Repetitive controller embeds an internal model within its structure to realize the repeating disturbance suppression or repeating reference tracking perfectly. A repetitive controller for tremor suppression was first proposed in [20] and the tremor of 3Hz was reduced by approximately 80% on unimpaired humans. In [21], the amplitude of the single peak frequency (2.5, 3 or 4 Hz) of the induced tremor was reduced greatly. The repetitive controller proposed in [15] increased single frequency tremor suppression by 43.3% compared with conventional filter based design.

While the above designs have shown feasible of FES based tremor suppression, they are based on the assumption that tremor is approximately a single frequency signal. However, it is an idealized simplification of the real scenario. Research results have shown that for different patients, tremor can have multiple frequencies, or even a frequency band [22], [23]. So the existing control schemes based on the single frequency assumption will limit the performance of tremor suppression and its practical application.

To address the above limitation, an FES based multi-periodic repetitive control for multiple frequency tremor suppression is proposed in this paper. First, we propose a nonlinear wrist musculoskeletal dynamics model with Hammerstein structure and an automatic parameter estimation procedure which can be easily utilized to the experimental and clinical applications. Then, a linearizing controller is proposed to linearize the nonlinear wrist dynamics and a multi-periodic repetitive controller is put forward to suppress multiple frequency tremor. The stability of the closed loop system is analyzed. Two different methods for implementing the proposed multi-periodic repetitive controller are also presented. Finally, the simulation and experiments of unimpaired participants and one intention tremor patient are carried out to verified the effectiveness of the proposed method. The obtained results validate that the proposed control method can improve the multiple frequency tremor suppression performance greatly.

This paper substantially extends our preliminary results in 21st IFAC World Congress 2020 [24] by (i) developing a new control algorithm, namely gradient based multi-periodic repetitive control algorithm, (ii) including a rigorous proof of the stability of the closed-loop system, and furthermore, (iii) adding new tremor suppression experiments on intention tremor patient to verify the proposed control methods.

The rest of the paper is arranged as follows: Section II establishes a parameterized nonlinear wrist musculoskeletal model with Hammerstein structure. A controller combining linearizing controller and multi-periodic repetitive control is put forward in Section III. Simulation testing and experimental verification are presented in Section IV. Finally, Section V summarizes the paper and draws conclusions and future work.

II. Musculoskeletal Model and its Parameterization

The purpose of this paper is to develop a feedback multi-periodic repetitive control system to suppress multiple frequency wrist tremor by the means of FES. In this research, we focus on the wrist tremor suppression about intention tremor patient. Intention tremor is a kind of kinetic tremor with a frequency range of 2-5Hz and is generally occurs in the patients with multiple sclerosis when they perform some movement tasks, such as to reach a target [25]. The diagram of the overall system is shown in Fig. 1. The real-time angle

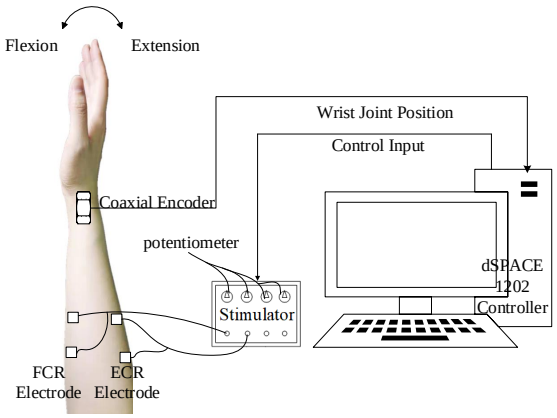

Fig. 1. Diagram of the wrist tremor suppression system.

data of wrist flexion and extension collected by the encoder is transmitted to dSPACE to realize the direct interface with Matlab/Simulink. According to the error between designated tracking reference position and the real tracking position, the controller is designed to generate the appropriate FES signals. Then the stimulator produces electrical signals to stimulate the corresponding muscles, i.e. flexor carpi radialis (FCR) and extensor carpi radialis (ECR), such that the muscles contract in anti-phase with tremor motion to reduce the tremor amplitude. To achieve this purpose, the model of wrist musculoskeletal dynamics is developed in this section. The dynamic model is then simplified and parameterized to facilitate the parameter identification and controller design.

The wrist musculoskeletal model includes the muscle model and the skeletal model. The dynamics of muscle is very complex and to fully capture it requires including all the factors, e.g. muscle velocity. There are models to captures these, e.g. Hill-Huxley model [26], [27]. These models however are very complex which undermines their application in control design. For the FES based tremor suppression system, the ranges and velocities of the joint are small. Additionally, muscle stretching and shortening have minor effect on the generated force because of the low amplitude and frequency of tremulous motion (2-5Hz, intention tremor) [28]. Thus, the fore-length and force-velocity of Hill-type model can be neglected and the dynamic component is almost uniformly represented by a Hammerstein structure. In this paper, we choose the nonlinear Hammerstein model to represent human muscles, which is a popular choice for controller design due to its simple model structure. The Hammerstein model is composed of the

nonlinear static muscle isometric recruitment curves (IRCs) and linear contraction dynamics [29]. The skeletal model can be regarded as rigid body dynamics (RBD).

The structure of the electrically stimulated wrist musculoskeletal model is shown in Fig. 2, where $u_{\rm fcr}(k)$, $u_{\rm ecr}(k)$ represent the electrical stimulations acting on the muscles. $f_{\rm fcr}(u_{\rm fcr})$ and $f_{\rm ecr}(u_{\rm ecr})$ are the IRCs of the corresponding muscles respectively. $w_{\rm fcr}(k), w_{\rm ecr}(k)$ are the steady-state isometric muscle torques. $d_{\rm fcr}(k)$ and $d_{\rm ecr}(k)$ are the tremor signals. $G_{\rm fcr}(z)$ and $G_{\rm ecr}(z)$ are linear muscle contraction dynamics. $\tau(k) = \tau_{\rm fcr}(k) - \tau_{\rm ecr}(k)$ is the muscle moment. $G_{\rm RBD}$ represents the wrist skeletal dynamics. $y(k)$ is the joint angle of wrist flexion and extension motion.

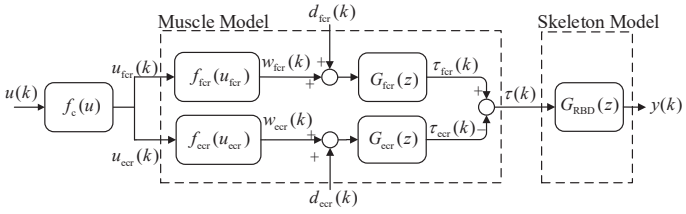

Fig. 2. Electrically stimulated wrist musculoskeletal model.

Taking into consideration of the co-activation, which refers to the simultaneous activation of antagonist and agonist muscles and modulates mechanical impedance to maintain the stability of wrist joint during voluntary movement, the function $f_{\rm c}(u(k)) = (u_{\rm fcr}(k) \quad u_{\rm ecr}(k))^T$ mapping a single control input $u(k)$ to the electrical stimulation signals applied to FCR and ECR can be formulated as follows

$$\begin{aligned} u_{\rm fcr}(k) &= \begin{cases} u_{\rm fcr,co} + u(k), & u(k) \geq 0, \\ u_{\rm fcr,co}, & u(k) < 0, \end{cases} \\ u_{\rm ecr}(k) &= \begin{cases} u_{\rm ecr,co}, & u(k) \geq 0, \\ u_{\rm ecr,co} - u(k), & u(k) < 0, \end{cases} \end{aligned} \tag{1}$$

where $u_{\rm fcr,co}$ and $u_{\rm ecr,co}$ are the co-activation levels of FCR and ECR muscles respectively.

The typical isometric recruitment curve (IRC) of muscles is a S-function with dead-zone region and saturation region, as shown in Fig. 3 (a). Letting $u_{\rm fcr,zo} = u_{\rm fcr,co}$ and $u_{\rm ecr,zo} = u_{\rm ecr,co}$, $f_{\rm fcr}(u_{\rm fcr}(k))$ and $f_{\rm ecr}(u_{\rm ecr}(k))$ can be transformed into a single nonlinear mapping function $f(u(k))$ without dead zones, as shown in Fig. 3 (b).

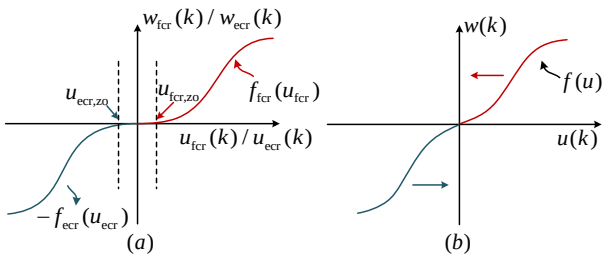

Fig. 3. (a) Typical IRCs where $u_{\rm fcr,zo}$ and $u_{\rm ecr,zo}$ are the dead zones of IRCs. (b) Modified IRC without dead zones.

The total muscle torque $w(k)$ then can be related to $u(k)$ by the following static mapping

$$f(u(k)) := \begin{cases} f_{\rm fcr}(u(k) + u_{\rm fcr,co}) - f_{\rm ecr}(u_{\rm ecr,co}), \\ \quad u(k) \in [0, u_{\max} - u_{\rm fcr,co}], \\ -f_{\rm ecr}(u_{\rm ecr,co} - u(k)) + f_{\rm fcr}(u_{\rm fcr,co}), \\ \quad u(k) \in [u_{\rm ecr,co} - u_{\max}, 0]. \end{cases} \tag{2}$$

where $u_{\max}$ is the maximum electrical stimulation level in FES-based tremor suppression. The maximum pulse width is set to 300μs to avoid uncomfortable muscle contraction [30]. It is obvious that $f(u)$ is a continuous and monotonic increasing S-function without saturation over the domain $[u_{\rm ecr,co} - u_{\max}, u_{\max} - u_{\rm fcr,co}]$. The equivalent static recruitment nonlinearity can be then expressed as

$$f(u(k)) = \begin{cases} \alpha_0 \left(\frac{e^{\alpha_1 u(k)} - 1}{e^{\alpha_1 u(k)} + \alpha_2} \right), & u \in [0, u_{\max} - u_{\rm fcr,co}], \\ -\beta_0 \left(\frac{e^{\beta_1 (-u(k))} - 1}{e^{\beta_1 (-u(k))} + \beta_2} \right), & u \in [u_{\rm ecr,co} - u_{\max}, 0], \end{cases} \tag{3}$$

where α_i, β_i $(i = 0, 1, 2)$ are the nonlinear scalar parameters to be identified for FCR and ECR muscles respectively.

Noting that similar muscle groups have similar linear contraction dynamics [31], we assume that wrist flexor and extensor have similar biophysical properties, that is, $G_{\rm fcr}(z) \approx G_{\rm ecr}(z)$, which is denoted as $G_{\rm L}(z)$. The rigid body dynamics $G_{\rm RBD}(z)$ is commonly considered to exhibit linear stiffness and damping [32], [33]. The equivalent linear musculoskeletal model can be obtained as following

$$P(z) = G_{\rm L}(z) G_{\rm RBD}(z) = \frac{B(z^{-1})}{A(z^{-1})}, \tag{4}$$

where $B(z^{-1})$ and $A(z^{-1})$ are numerator and denominator of the linear wrist model respectively, which are nominal polynomials in the form of

$$\begin{aligned} B(z^{-1}) &= b_1 z^{-1} + \cdots + b_{n_b} z^{-n_b}, \\ A(z^{-1}) &= 1 + a_1 z^{-1} + \ldots + a_{n_a} z^{-n_a}, \end{aligned} \tag{5}$$

where n_a, n_b are the orders of $A(z^{-1})$ and $B(z^{-1})$ respectively, $b_1, \cdots, b_{n_b}$ and $a_1, \cdots, a_{n_a}$ are parameters to be identified. In Section IV, the identification of the nonlinear and linear parameters in the wrist musculoskeletal model will be described in detail.

III. Control Development

The tremor signal can be regarded as multi-frequency disturbance acting on the wrist musculoskeletal model. In this section, a combined linearization control and feedback multi-periodic repetitive control strategy is proposed to suppress multiple frequency wrist tremor. The linearizing controller is to cancel the effect of the muscle nonlinearities. The multi-periodic repetitive control embeds multi-periodic signal generator in the internal model control loop to completely suppress the multi-periodic disturbance. The closed feedback control diagram is shown in Fig. 4, where $r(k)$ is the designated tracking reference position, $y(k)$ is the actual output angle of wrist flexion and extension motion, $e(k)$ is the deviation between the actual wrist flexion and extension motion position

and the designated tracking reference position. The antagonist and agonist muscle pair have input from the same oscillatory source at the tremor frequency [34], [35]. Therefore, $d(k)$ is assumed as an equivalent tremor signal as a result of $d_{\text{ecr}}(k)$ and $d_{\text{fcr}}(k)$, acting on the wrist muscle. $C(z)$ is the feedback multi-periodic repetitive controller and $\bar{w}(k)$ is the output of repetitive controller. $f^{-1}(\bar{w})$ is the linearizing controller.

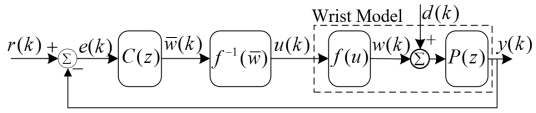

Fig. 4. The closed-loop feedback control diagram

A. Controller design

1) Linearizing controller: Because the electrically stimulated musculoskeletal model has complex nonlinear factors and the nonlinearity is mainly manifested in static isometric recruitment characteristic, the linearization control method is used to linearize the model where the recruitment nonlinearity $f(u)$ is cancelled by the function of $f^{-1}(\bar{w})$. The inverse nonlinear function is constructed as

$$f^{-1}(\bar{w}) = \begin{cases} \frac{1}{\alpha_1} ln\left(\frac{\alpha_0+\alpha_2\bar{w}}{\alpha_0-\bar{w}}\right), & \bar{w} > 0 \\ -\frac{1}{\beta_1} ln\left(\frac{\beta_0-\beta_2\bar{w}}{\beta_0+\bar{w}}\right), & \bar{w} \leq 0, \end{cases} \tag{6}$$

which is obtained directly from (3).

2) Multi-periodic repetitive controller: Multi-periodic repetitive control is a control strategy based on the multi-periodic internal model principle. The repetitive controller embeds the internal model of multiple frequency disturbance in the control structure to eliminate the disturbance accurately. The diagram of the proposed multi-periodic repetitive controller is shown in Fig. 5, where $K_p, p = 1, ...n$ is the gain of each repetitive control loop, $H(z)$ is the compensator and $Q(z)$ is the robust low pass filter. This multi-periodic repetitive controller is inspired by [36] and has a simplified structure and is easy to design.

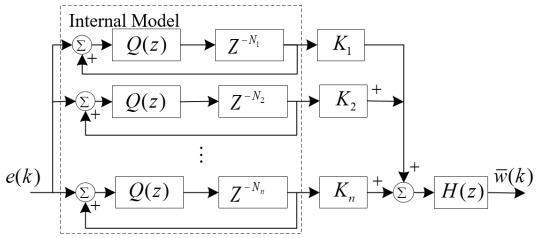

Fig. 5. The diagram of multi-periodic repetitive controller $C(z)$

From Fig. 4 and Fig. 5, the multi-periodic repetitive controller is

$$u(k) = f^{-1}(C(z)e(k)), \tag{7}$$

where $C(z)$ takes the form of

$$C(z) = (\sum_{p=1}^{n} \frac{Q(z)z^{-N_p}}{1-Q(z)z^{-N_p}} K_p) H(z). \tag{8}$$

with $G_{\text{IM}p}(z) = \frac{Q(z)z^{-N_p}}{1-Q(z)z^{-N_p}}$ $(p = 1, \cdots, n)$ being the p^{th} internal model, where $N_p = \frac{T_p}{T_s}$ is the number of samples in a period, T_p is the periodic signal and T_s is the sampling period. In order to obtain robustness of the repetitive control system under modeling uncertainty, $Q(z)$ is chosen as a zero phase low pass filter with unity gain at low frequencies as follows [37],

$$Q(z) = \frac{\sum_{i=0}^{N_p/2} \alpha_i z^i + \sum_{i=1}^{N_p/2} \alpha_i z^{-i}}{2\sum_{i=1}^{N_p/2} \alpha_i + \alpha_0}, \tag{9}$$

where $\alpha_i (i = 0, 1, 2, ..., N_p/2)$ are coefficients to be designed. The compensator $H(z)$ is set according to the characteristics of the model $P(z)$ to improve the stability and dynamic performance of the system. $H(z)$ can be expressed as

$$H(z) = \frac{c_1 z^{n-1} + c_2 z^{n-2} + \cdots + c_m z^{n-m} + \cdots + c_n z^0}{z^{n-m}}. \tag{10}$$

It contains n zeros whose locations are to be determined by coefficients $c_1, c_2 \cdots, c_n$, and $n - m$ poles are introduced at the origin.

B. Stability analysis

Theorem 1. Under the multi-periodic repetitive controller (7), the closed-loop control system shown in Fig. 4 is asymptotically stable and the multi-periodic disturbances can be rejected if the control gains K_p, the compensator $H(z)$ and robust low pass filter $Q(z)$ are chosen such that the roots of the following characteristic polynomial of the closed-loop control system are all within the unit circle

$$1 + P(z)H(z)\sum_{p=1}^{n} \frac{Q(z)z^{-N_p}}{1-Q(z)z^{-N_p}} K_p = 0. \tag{11}$$

Especially, for the ideal choice of $H(z) = P^{-1}(z)$ and $Q(z) = 1$, a sufficient condition for the choice of K_p is given by

$$\sum_{p=1}^{n} K_p < 2, K_p > 0, p = 1, 2, ...n. \tag{12}$$

Proof: The proof is shown in Appendix A.

C. Two repetitive controller design methods

In practice, it is impossible to exactly achieve $H(z)P(z) = 1$ because of the model uncertainty and the possible presence of zeros outside the unit circle. The following two methods, frequency modified inverse multi-periodic repetitive control (FMI-MP-RC) algorithm and gradient-based multi-periodic RC (GB-MP-RC) algorithm will be used to construct the compensator $H(z)$.

1) FMI-MP-RC algorithm: The parameters $\mathbf{c} = [c_1 \quad c_2 \cdots \quad c_n]^T$ in (10) can be appropriately selected to minimize the following cost function

$$J = \sum_{j=0}^{N_p} [1 - P(e^{i\omega_j T})H(e^{i\omega_j T})]W_j[1 - P(e^{i\omega_j T})H(e^{i\omega_j T})]^*, \tag{13}$$

so as to make $H(e^{i\omega_j T})$ as an approximation frequency response of $P^{-1}(e^{i\omega_j T})$, where ω_j is a discrete set of frequencies selected zero to Nyquist, and W_j is the weighting factor to the $j-$th frequency. It is shown in [38], W_j usually can be set to one. Let $P(e^{i\omega_j T}) = M_P(\omega_j)e^{i\varphi_P(\omega_j)}$. Substituting (10) into the cost function (13), we get a set of linear equations

$$\varphi = D^{-1}\Gamma, \tag{14}$$

where

$$D = \sum_{j=0}^{N_p} W_j M_P^2(\omega_j)\Theta, \tag{15}$$

$$\Gamma = \sum_{j=0}^{N_p} W_j M_P(\omega_j) \begin{bmatrix} \cos((m-1)\omega_j T + \varphi_P(\omega_j)) \\ \cos((m-2)\omega_j T + \varphi_P(\omega_j)) \\ \cdots \\ \cos((m-n)\omega_j T + \varphi_P(\omega_j)) \end{bmatrix}, \tag{16}$$

$$\Theta = \begin{bmatrix} 1 & \cos(\omega_j T) & \cdots & \cos((n-1)\omega_j T) \\ \cos(\omega_j T) & 1 & \cdots & \cos((n-2)\omega_j T) \\ \vdots & \vdots & \ddots & \vdots \\ \cos((n-1)\omega_j T) & \cos((n-1)\omega_j T) & \cdots & 1 \end{bmatrix}. \tag{17}$$

Choosing appropriate m and n in (10) can generate various patterns for the optimized zero locations of the compensator $H(e^{i\omega T})$, which makes $H(e^{i\omega T})$ approximate $P^{-1}(e^{i\omega T})$. The parameters $\mathbf{c}$ can be obtained by solving the equation (14) when (12) is satisfied.

2) GB-MP-RC algorithm: The GB-MP-RC algorithm is based on the contraction mapping technique [39] and $H(z)$ can be constructed as

$$H(z) = \gamma P^*(z), \tag{18}$$

where $\gamma > 0$ is a scalar gain, the $(\cdot)^*$ denotes the complex conjugate and the non-causal plant adjoint operator satisfying $P^*(z) = P(z^{-1})$ with

$$P(z^{-1}) = \sum_{j=1}^{N_p} h_j z^{N_p - j}, \tag{19}$$

in which h_j are the Markov parameters of $P(z)$. By choosing $m = n = N_p$, (10) becomes

$$H(z) = \sum_{j=1}^{N_p} c_j z^{N_p - j} = \gamma \sum_{j=1}^{N_p} h_j z^{N_p - j}. \tag{20}$$

Substitute (20) into (11), we have

$$1 + \gamma P(z)P^*(z) \sum_{p=1}^{n} G_{\mathrm{IM}p}(z)K_p = 0, \tag{21}$$

and the real part of (21) is

$$1 + Re(\gamma P(z)P^*(z) \sum_{p=1}^{n} G_{\mathrm{IM}p}(z)K_p) = 0, \tag{22}$$

then

$$1 + \gamma |P(z)|^2 Re(\sum_{p=1}^{n} G_{\mathrm{IM}p}(z)K_p) = 0. \tag{23}$$

For any z outside the unit circle, we can show $Re(G_{\mathrm{IM}p}(z)) \geq -\frac{1}{2}$ is satisfied (see the appendix A for the proof). Then we have

$$\begin{aligned} &\gamma |P(z)|^2 Re(\sum_{p=1}^{n} G_{\mathrm{IM}p}(z)K_p) \\ &\geq -\frac{1}{2}\gamma \|P(z)\|_\infty^2 \sum_{p=1}^{n} K_p, \forall |z| \geq 1. \end{aligned} \tag{24}$$

If γ is chosen such that

$$0 < \gamma < \frac{2}{\|P(z)\|_\infty^2 \sum\limits_{p=1}^{n} K_p}, \tag{25}$$

the real part of characteristic polynomial satisfies

$$\begin{aligned} &1 + \gamma |P(z)|^2 Re(\sum_{p=1}^{n} G_{\mathrm{IM}p}(z)K_p) \\ &\geq 1 - \frac{1}{2}\gamma \|P(z)\|_\infty^2 \sum_{p=1}^{n} K_p > 0, \forall |z| \geq 1 \end{aligned} \tag{26}$$

i.e. the characteristic polynomial

$$1 + \gamma |P(z)|^2 Re(\sum_{p=1}^{n} G_{\mathrm{IM}p}(z)K_p) \neq 0, \forall |z| \geq 1. \tag{27}$$

Therefore, if (25) is satisfied, all the roots of the characteristic polynomial are within the unit circle and thus the closed loop system is asymptotically stable.

IV. Experimental verification

In this section, an experimental platform for FES-based wrist multi-frequency tremor suppression is established and a systematic experimental approach is proposed to verify the effectiveness of the proposed methods. Ethical approval is obtained from the Zhengzhou University, China (No.ZZURIB2019-004). Written informed consent is given to all intention tremor patients and unimpaired participants.

All the participants need to meet the following criteria: 1) The upper limbs of the subjects have certain ability of voluntary movement; 2) No diagnosed dermatosis and no allergic to electrode self-adhesive; 3) Normal cognitive/vision and hearing function; 4) No pacemaker or attached electronics; 5) In order to make sure there is no voluntary effort to suppress tremor during the experiments, all the participants need to completely relax their right arm and the tremor suppression is driven by electrical stimulation signals instead of self generating muscle torque. A total number of 9 subjects were recruited at different stages: 4 intention tremor patients (patients 1-4, two male and two female) for tremor data collection and

analysis, 4 unimpaired subjects (participants 1-4, three male and one female) for testing of the proposed design (a critical stage before any clinical trial), and an intention tremor patient (male) to evaluate the design's performance.

To make the experimental process more clearly, the flow chart of the experimental protocol can be found in Fig. 6. The experimental set-up is divided into two parts: parameter identification of wrist musculoskeletal model and tremor suppression tests. Furthermore, in order to prevent muscle fatigue, participants are regularly asked if they feel muscle fatigue at each experimental phase. If the participants feel tired, the experiment will be stopped immediately.

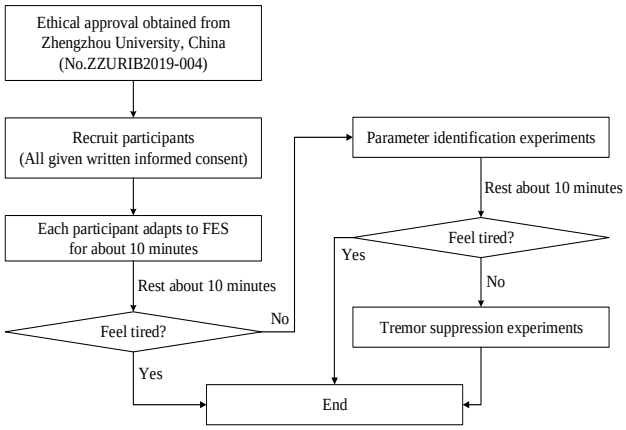

Fig. 6. The flow chart of experimental protocol

In this section, the experimental platform is firstly illustrated in detail. Then, the parameters identification process of the participant's musculoskeletal model is introduced. Thirdly, comparative simulation testing is given to demonstrate the feasibility and effectiveness of the proposed control algorithm. Finally, experimental verification results through comparative experiments on the experimental platform are presented.

A. Experimental set-up

The experimental platform can realize the parameter identification of wrist musculoskeletal model and tremor suppression in wrist flexion and extension plane on participants. It is modified on a commercially available wheelchair (Yuwell H062). As shown in Fig. 7 (a), an arm bracket is designed on the right side of the wheelchair, and the movement range of the arm bracket is limited between plus and minus 80 degrees centered on the natural placement of the arm. During the experimental process, two pairs of surface electrodes (4cm×4cm) are attached to FCR and ECR muscles of the participant respectively (In Fig. 7 (b)). The participant is sited comfortably and relaxedly on the wheelchair of the platform with the right forearm on the arm bracket and the right hand in the middle of the U-shaped splint. The forearm of the participant is fixed with mould to generate wrist flexion and extension plane motion and to prevent any movement of the elbow. A fan-shaped angle ruler is designed on the outside of the bracket, and the angle is marked on the angle ruler, which is convenient for participants to track the designated tracking position. The real-time tracking position is obtained by the encoder (E6B2-CWZ6C) because the shaft of encoder and the rotating shaft of bracket are connected by a gear with a diameter ratio of 1:1. The dSpace platform (Microlabbox 1202) provides support for development and verification of control algorithm through real-time transmission of wrist position data and control signals, and control signal is implemented by four channel functional electrical stimulator (Odstock Medical). The implementation of the above hardware modules forms the closed-loop of the tremor suppression control system.

The frequency, current amplitude and maximum pulse width of the stimulation signal is set to 40Hz (biphasic and asymmetrical PWM sequences), 20mA and 300μs respectively in this study. According to the response of each participant to the electric stimulation signal, the amplitude of PWM waveform can be adjusted by using the potentiometer of each channel on the stimulator.

It is worth pointing out that for this type of research, conducting feasibility test on healthy subjects is an essential step before clinical trials. Therefore, a DC-motor (BJ VDM08SGN24-60-1800/JB5G12T) is embedded in the experimental platform and the tremor signals can be simulated by the motor. The rotation axis of the bracket is coaxial with the motor, so the bracket can be directly driven to swing according to the rotation of the motor. As a result, the wrist of unimpaired participants can produce involuntary motion, i.e. wrist flexion and extension tremor. This type of tremor generator makes participants feel more comfortable than the electrical pulse signals directly stimulating muscles.

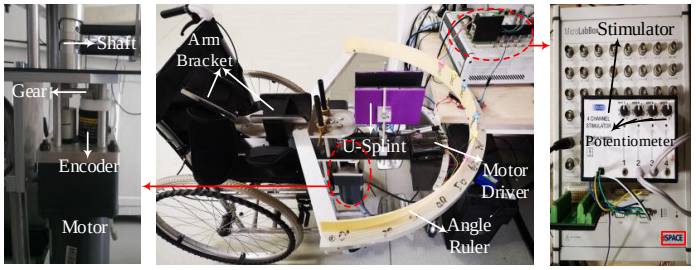

(a)

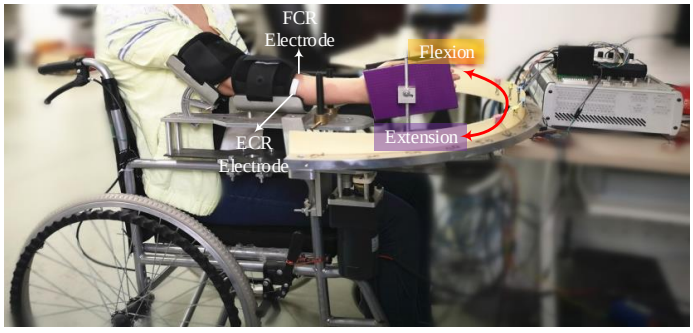

(b)

Fig. 7. (a) Wrist tremor suppression experimental platform. (b) The platform limits wrist movement in the plane of flexion and extension

B. Model identification

In this subsection, parameters identification of the electrically stimulated wrist musculoskeletal model with Hammerstein structure will be explained. The parameter identification procedure includes two steps, nonlinear parameters estimation and linear parameters identification. The identification process is simple and very suitable for clinical application. Note that this paper considers intention tremor which is a kind of kinetic tremor and increases in amplitude especially when limb approaches a specific target. When the intention tremor patient does the parameter identification experiments, the wrist of the patient is kept relaxing, so tremor motion is insignificant against the electrical stimulation motion. Therefore, the tremor can be neglected during model identification.

1) Nonlinear parameters estimation: Peak impulse response method is used to estimate IRCs by mapping the peak value of muscle impulse response to a single stimulus pulse [40]. The stimulus pulse includes 6 different pulse widths, that is, 50μs, 100μs, 150μs, 200μs, 250μs and 300μs. The minimum pulse width 50μs, i.e. value of $u_{\mathrm{ecr,zo}}$ or $u_{\mathrm{fcr,zo}}$, is selected according to the muscle activation characteristics. We estimate this value using experiments by increasing the electrical stimulation input level until the wrist angle changes. That corresponding FES levels would be the values of $u_{\mathrm{ecr,zo}}$ and $u_{\mathrm{fcr,zo}}$. We have done a large number of experiments and the values of $u_{\mathrm{ecr,zo}}$ and $u_{\mathrm{fcr,zo}}$ are all around 50μs. Therefore, 50μs is chosen in practice. The maximum pulse width is set to 300μs to avoid uncomfortable muscle contraction [30]. Each pulse width repeats five times, so one test consists of 30 stimulus pulses. The final result is obtained by the average of the five responses for each pulse width. During the nonlinear parameter identification, the output of muscle torque is not directly measured. The joint angle is measured instead as the muscle torque and the joint angle are related by a linear transfer function (i.e. $P(z)$ in Fig. 4) and thus at steady state they are linked by a constant number. Therefore, the measured angle can reflect the muscle torque (up to a constant scaling). Note that it is not necessary to know this scaling constant as the IRCs are normalised later in (28).

Using the input pulse signals u_i and the (indirectly) measured output w_i, the least squares nonlinear curve fitting procedure is employed to identify the nonlinear parameters. The whole identification process takes less than two minutes. The activation level is then normalized in the range 0-1, which is acquired by the following formula

$$w_{\mathrm{Act}} = \frac{w_i}{w_{max}}, \tag{28}$$

where the w_{max} is maximum (indirectly) measured output torque when u_i is chosen as 300μs. As a representative example, the FCR and ECR muscles' IRCs of a participant (Participant No.1 which will be introduced later) obtained by this method are shown in Fig. 8. As can be seen, the IRCs are continuous and monotonic (thus the exact inverses can be obtained for later linear parameter identification and controller design).

2) Linear parameters identification: In order to obtain the test data used to identify the parameters of the musculoskeletal model $P(z)$, we use input signals u comprising a set of sine waves with different frequencies ranging from 0.2Hz to 4Hz and 300μs pulse width, i.e. $u_i(k)$ = 300sin$(f_i k)$ where f_i=0.2, 0.4, $\cdots$ 4Hz. The patient's wrist is driven by input electrical stimulation signals and the angle sensor will collect the corresponding wrist position y. We need to estimate linear parameters based on the input/output data set $[u, y]$, given we have already known the nonlinear IRCs parameters. The experimental protocol of the linear parameter identification is described in Algorithm 1.

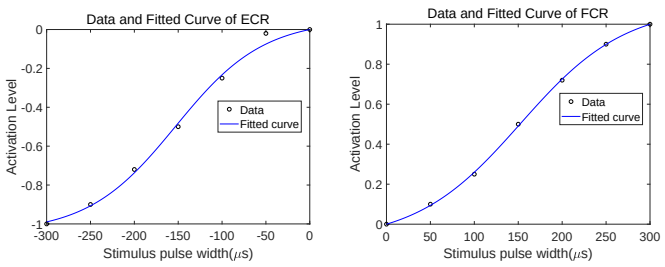

Fig. 8. The ECR and FCR muscles IRCs of Participant No.1

Algorithm 1 Experimental test procedure for linear parameters identificaiton

Input: a set of stimulation signals $u_i, i = 1, 2, \cdots, n$
Output: angle response $y_i, i = 1, 2, \cdots, n$
Step 1: set $i = 1$
Step 2: Apply stimulation signal u_i while relaxing voluntary effort and recording y_i
Step 3: increment i and go to step 2

The estimation of linear parameters can be obtained by the least square identification algorithm. Each linear identification process lasts about two minutes and each participant need to be identified four times. The obtained input/output data are divided into two groups, one as training set and the other as validation set. The goal of validation is to obtain the wrist model by input/output data set and the goal of cross-validation is to test the model's ability to predict new data that was not used in estimating it. The first two sets of input/output data are used to identify a model and the remaining other two sets are used for validating the model on a new input/output set. In Table I, the fitness of validation is expressed in terms of best fit rate (BFR), defined as follows,

$$\mathrm{BFR} = 100(1 - \frac{\|y - \hat{y}\|_2}{\|y - \bar{y}\|_2})\%, \tag{29}$$

where y is the measured output, $\hat{y}$ denotes the simulated model output. The mean value of y is denoted by $\bar{y}$. The higher values of BFR give rise to higher accuracy but also tend to require a higher model order. Therefore, the parameters of n_a and n_b (orders of $A(z)$, $B(z)$ in $P(z)$) are chosen from 4 to 10. As a representative example, the best fit rate of Participant No.1 is shown in Table. I.

It can be seen from Table I that the best fit rate of relative lower order model is 63.06% ($n_a = 4$ and $n_b = 4$), and the

TABLE I
THE BEST FITTING VALUES OF PARTICIPANT NO.1

n_a		n_b 4	5	6	8	10
4	V	63.06%	63.64%	65.45%	67.46%	67.48%
	CV	60.25%	57.08%	57.12%	59.24%	60.95%
5	V	64.15%	66.04%	66.43%	67.79%	67.94%
	CV	58.24%	58.08%	55.98%	55.21%	56.26%
6	V	63.99%	65.89%	66.9%	67.46%	67.68%
	CV	55.37%	55.66%	55.02%	52.54%	52.85%
8	V	62.03%	63.76%	64.81%	65.67%	65.98%
	CV	53.34%	53.56%	53.15%	51.18%	50.88%
10	V	58.96%	60.57%	61.58%	62.56%	63.09%
	CV	53.96%	54.22%	53.83%	51.87%	51.49%

V: Validation, CV: Cross Validation

highest best fit rate of relative higher order model is 67.94% ($n_a = 5$ and $n_b = 10$). The changes in best fit rate are not significant when n_a and n_b are varied from 4 to 10. Therefore, in order to reduce the identification computation and benefit the controller design, $n_a = 4$ and $n_b = 4$ are chosen in this paper.

C. Simulation testing

In this subsection we carry out simulation testings using Participant No.1's identified model to verify the feasibility and effectiveness of the proposed FMI-MP-RC algorithm and GB-MP-RC algorithm for wrist multi-frequency tremor suppression. The results of FMI-MP-RC algorithm, GB-MP-RC algorithm, frequency modified inverse single periodic RC (FMI-SP-RC) algorithm [15] and the conventional PI high-pass filter (PI-HF) based control algorithm [17] will be compared.

1) Simulation testing-Phase I: In simulation testing, the multi-frequency disturbance $d(z)$ is set to superposition of two sinusoidal signals with the frequencies of $f_1 = 2$Hz, $f_2 = 2.5$Hz and the amplitude of 1 and 0.4 respectively. The sample period T_s is 0.005s. The delay period of the repetitive controller is $N_1 = 100$ and $N_2 = 80$. The gains of the RC controller are $K_1 = K_2 = 0.5$ and $Q(z) = 1$. The internal model of FMI-SP-RC algorithm includes single frequency tremor signal with the frequency is 2Hz, which is the major frequency component. For the two parameters m and n in the RC algorithm, the optimal value is obtained by minimize the cost function (13). The choice of γ should satisfy the formula (25). The optimized parameters of PI-HF regulator is determined by trial and error method. The filter order and cut-off frequency of high pass Butterworth filter are $6th$ and $1.2Hz$ respectively. We set the voluntary wrist movement reference $r(z)$ equals to zero and the output $y(z)$ will trace the reference signal under the effect of disturbance $d(z)$. The orders and parameters of the Participant No.1' musculoskeletal model $f(u)$ and $P(z)$ are obtained by experimental platform with $\alpha_0 = 1.0449, \alpha_1 = 0.0199, \alpha_2 = 21.1254, \beta_0 = 1.0050, \beta_1 = 0.0217, \beta_2 = 20.1696, a_1 = -1.085, a_2 = -0.319, a_3 = 0.04332, a_4 = 0.3629, b_1 = 0.00721, b_2 = -0.009066, b_3 = -0.003751, b_4 = 0.005807$.

The following performance indicators are used to quantify the performance of each control algorithm on tremor suppression and intuitively analyze the advantages of FMI-MP-RC algorithm and GB-MP-RC algorithm over the other two algorithms.

(1) Root mean square error (RMSE),

$$\mathrm{RMSE} = \sqrt{\frac{1}{n}\sum_{i=0}^{n}(r_i - y_i)^2}, \tag{30}$$

where y_i is the output signal, r_i is the reference signal and n is the total sample numbers in simulation test. The smaller the RMSE value, the better the signal tracking, which means the better performance of multiple frequency tremor suppression.

(2) Tremor suppression rate (TSR)

$$\begin{aligned}\mathrm{TSR} &= (1 - \frac{\triangle y}{\triangle v}) \times 100\% \\ &= (1 - \frac{\sqrt{\frac{1}{n}\sum_{i=0}^{n}(r_i - y_i)^2}}{\sqrt{\frac{1}{n}\sum_{i=0}^{n}(r_i - v_i)^2}}) \times 100\%\end{aligned} \tag{31}$$

where $\triangle y$ is the deviation between the input signal r_i and output y_i. v_i is the effect of tremor signal on the tracking angles (i.e. without using any controller). $\triangle v$ is the deviation between input signal r_i and v_i. The ratio of $\triangle v$-$\triangle y$ to $\triangle v$ is the tremor attenuation performance.

Simulation results are shown in Table. II with different control algorithms and different controller parameters.

TABLE II
SIMULATION RESULTS WITH DIFFERENT CONTROLLER PARAMETERS

Controller Type	Controller Parameters	RMSE(°) (0-20s)	RMSE(°) (15-20s)	TSR (0-20s)	TSR (15-20s)
FMI-MP-RC	m=41,n=35	0.0454	1.1460×10^{-14}	94.04%	100%
	m=53,n=47	0.0439	1.0308×10^{-14}	94.23%	100%
	m=61,n=55	0.0358	9.9136×10^{-15}	95.30%	100%
GB-MP-RC	$\gamma = 65$	0.0569	4.4592×10^{-5}	92.52%	100%
	$\gamma = 85$	0.0527	3.7876×10^{-5}	93.08%	100%
	$\gamma = 115$	0.0501	3.5135×10^{-5}	93.42%	100%
FMI-SP-RC	m=41,n=35	0.3087	0.3067	59.47%	59.61%
	m=53,n=47	0.2947	0.2929	61.31%	61.54%
	m=61,n=55	0.2820	0.2799	62.97%	63.24%
PI-HF	K_P=60,K_I=60	0.4638	0.4554	40.20%	41.81%
	K_P=65,K_I=65	0.4405	0.4385	42.15%	43.27%
	K_P=70,K_I=70	0.4291	0.4242	43.66%	44.03%

As shown in Table. II, the RMSE (0-20s) of FMI-MP-RC algorithm is smallest among the four control algorithms, followed by the GB-MP-RC algorithm. The tremor amplitude is significantly reduced and the average TSR values of FMI-MP-RC algorithm and GB-MP-RC algorithm are up to 94.52% and 93.01% respectively, compared to 61.25% and 42.00% for the other two control algorithms. It means that the multi-periodic repetitive control algorithm (MP-RC) algorithms have the best tracking performance, that is, MP-RC method is more suitable for the suppression of multiple frequency tremor signal. In the last 5 seconds of simulation, the smallest RMSE values of FMI-MP-RC algorithm and GB-MP-RC algorithm are 9.9136×10^{-15} and 3.5135×10^{-5} respectively and the TSR values of the last 5 seconds of simulation testing are approximately 100%. However, the RMSE of the other two

algorithms in the last 5 seconds of simulation testing are significant. It demonstrates that the FMI-MP-RC algorithm and GB-MP-RC algorithm can almost completely suppress the multi-frequency tremor signal in steady state, while the other two controllers can't.

In order to illustrate the tracking performance more clearly, we depicts the tracking errors under different controllers in Fig. 9, where the parameters of the controllers are $m = 61, n = 55$ for FMI-MP-RC algorithm and FMI-SP-RC algorithm, $\gamma = 115$ for GB-MP-RC algorithm and $K_{\mathrm{P}} = 70$, $K_{\mathrm{I}} = 70$ for PI-HF algorithm. As illustrated by Fig. 9, the error signal of FMI-MP-RC algorithm fluctuates in the first few seconds, but converges to zero soon, and GB-MP-RC algorithm has similar results. While the error of FMI-SP-RC algorithm and PI-HF algorithm can not be eliminated completely with substantial residual.

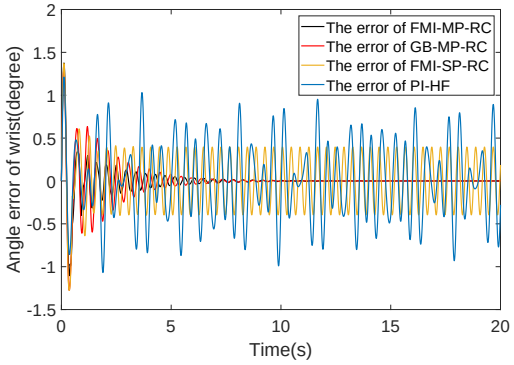

Fig. 9. The error time responses of the closed-loop system

The frequency analysis results of the error signals in the last few seconds of the simulation can be used to determine the suppression effect of the multiple frequency tremor signal by the four control algorithms. The frequencies of tremor signal are set to 2Hz and 2.5Hz. As indicated by Fig. 10, the frequency of steady-state error of FMI-MP-RC algorithm and GB-MP-RC are both zero, it means multi-periodic RC can suppress the multiple frequency tremor signal completely. The steady-state error frequency of FMI-SP-RC algorithm has only one peak value at 2.5Hz, which means that single internal model can not suppress multi-frequency tremor signal. The steady-state error frequency of PI-HF method has two peak values, which means the traditional filter based control algorithm can't suppress the multiple frequency tremor signal efficiently.

2) Simulation testing-Phase II: To demonstrate the robustness of the proposed multi-periodic repetitive control design, we have added another frequency (that is not considered by the controller). The amplitude and frequency of the disturbance signal are 0.3 and 2.7Hz respectively. All the settings are the same as before. The simulation results are shown in Table. III.

As illustrated in Table. III, despite the added signal close to the main frequency, both FMI-MP-RC algorithm and GB-MP-RC algorithm can still suppress the tremor efficiently (with average steady state TSR of 97.30% and 96.80% respectively). Representative results of the error signals under the proposed

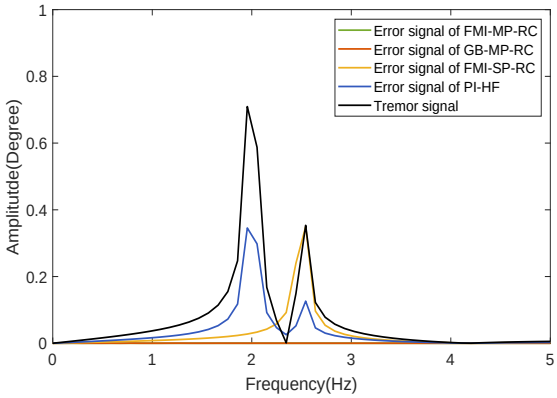

Fig. 10. The frequency analysis results

TABLE III
SIMULATION RESULTS WITH DISTURBANCE

Controller Type	Controller Parameters	RMSE(°) (0-20s)	RMSE(°) (15-20s)	TSR (0-20s)	TSR (15-20s)
FMI-MP-RC	m=41,n=35	0.0507	0.0216	93.35%	97.17%
	m=53,n=47	0.0431	0.0211	94.35%	97.23%
	m=61,n=55	0.0409	0.0190	94.63%	97.50%
GB-MP-RC	$\gamma = 65$	0.0633	0.0264	91.69%	96.53%
	$\gamma = 85$	0.0587	0.0247	92.29%	96.75%
	$\gamma = 115$	0.0552	0.0218	92.75%	97.13%

multi-periodic repetitive controllers ($m = 61, n = 55$ of FMI-MP-RC algorithm and $\gamma = 115$ of GB-MP-RC algorithm) are shown in Fig. 11. The tremor signals of these two proposed control methods are still significantly suppressed with only minor residual errors by adding the disturbance signal close to the main frequency, suggesting the proposed design has certain degree of robustness against model uncertainties.

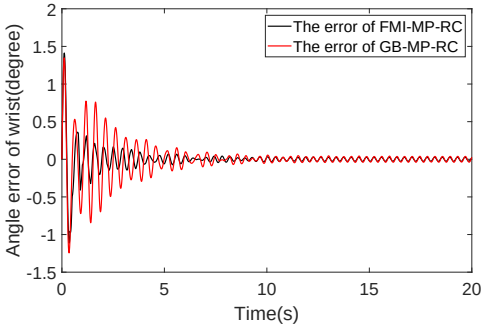

Fig. 11. The error time responses of the closed-loop system by adding another main frequency

D. Experiment verification

The experimental verification procedure is divided into three phases.

In Phase I, four intention tremor patients are recruited to perform data acquisition experiments of wrist flexion and extension motion. The purpose of this experiment is to verify that tremor is a multi-frequency signal, and the frequency range of intention tremor is 2-5Hz [25], [41].

In Phase II, the proposed control method to suppress wrist tremor is verified by experiments on four unimpaired participants by generating induced multi-frequency tremor signal from DC motor.

In Phase III, one intention tremor patient is recruited to perform the tremor suppression experiments.

1) Experimental results-Phase I: In order to better understand intention tremor spectrum and to make the simulation/experiments more close to the real cases, we collected the test data of the real intention tremor patients first. Four intention tremor patients were recruited from Rehabilitation Department, Fifth Affiliated Hospital of Zhengzhou University in July, 2019, including 2 males and 2 females, with an average age of 43.0 years and a standard deviation of 18.4. The dominant hand of all patients is the right hand. Because we only collect the patient's tremor data, we use the portable multi-functional physiological signal acquisition instrument (Biometrics Ltd), which is shown in Fig. 12.

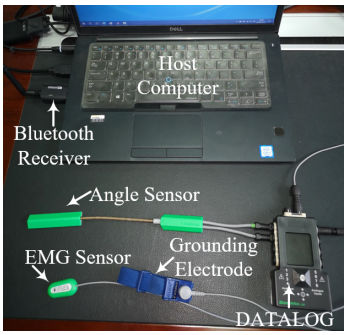

Fig. 12. Data acquisition experimental platform

In the experiment, tremor patients are required to move the cup to the designated position by flexing and extending wrist in the horizontal plane. During the whole process, the patients are in a relaxed state, and the angle data of the wrist joint in this task is collected. Fourier transform is used to analyze the data of wrist flexion and extension motion. Because of the voluntary motion frequency is less than 1Hz and the frequency range of involuntary motion is more than 1Hz [41], so 1Hz to 8Hz frequency spectrum of Patient No.1 is shown in Fig. 13.

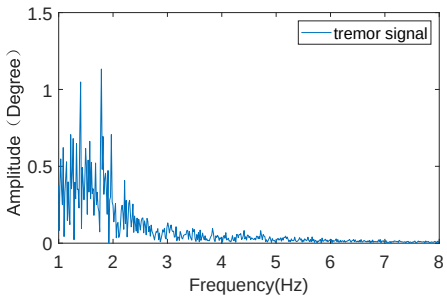

Fig. 13. The spectrum of wrist tremor (Patient No.1)

As shown in Fig. 13, the main components of intention tremor frequencies for Patient No.1 is less than 3Hz, and that the tremor signal is multi-frequency and has two main peaks with different amplitudes. The larger amplitude of the tremor frequency means the greater impact on the patient, so this paper mainly focuses on the suppression of the tremor signal of the main frequencies. The frequency spectrum analysis shows similar observations for the other three patients. The main tremor frequencies and amplitudes of four patients are shown in Table IV. In summary, tremor is manifested as multiple frequency signal by the results of experiment-Phase I.

TABLE IV
FREQUENCY ANALYSIS OF FOUR PATIENTS

Patient Number	Main Tremor Frequencies(Hz)	Amplitudes(°)
Patient No.1	1.4, 1.7	1.1, 1.2
Patient No.2	2.4, 2.5	3.8, 3.8
Patient No.3	1.5, 1.7	2.1, 2.8
Patient No.4	2.2, 2.4	3.3, 2.8

Remark 1: It is wroth noting that while the proposed repetitive controller design is based on the identified tremor frequencies, it is insensitive to small variations in tremor frequencies due to the continuity of the controller. The same controller can still work effectively (though with slightly sacrificed tremor suppression rate).

2) Experimental results-Phase II: In Phase II of the experiment, the following tests are performed on four unimpaired participants to fully evaluate the proposed control algorithm. This paper focused on intention tremor whose frequency range is 2-5 Hz [25], [41]. For the recruited tremor patients, the main tremor frequencies are all less than 3Hz. Therefore, in the experiments, the disturbance frequencies in the tremor are set to 2.5 Hz and 2Hz.

Test 1 (T1): Track designated reference trajectory autonomously without tremor and FES.

Test 2 (T2): Track designated reference trajectory with tremor but without FES (Tremor frequencies generated by motor are set to 2Hz and 2.5Hz).

Test 3 (T3): Track designated reference trajectory with both tremor and FES.

All participants are instructed to flex or extend their wrist voluntarily to track the designated reference trajectory in Test 1. Test 2 examines the effect of induced tremor on participant to perform the same tracking task. Test 3 examines the performance of tremor suppression by FES-based control algorithms mentioned above. Each participant must be accustomed to the designated tracking trajectory and functional electrical stimulation about ten minutes. In order to prevent muscle fatigue, each participant's electrical stimulation time is less than twenty minutes. Since Test 3 requires to be performed multiple times with different controllers and controller parameters, at least 10 minutes rest time is required between each test to prevent muscle fatigue [42]. In addition, during the experimental procedure, we constantly communicate with the participants to ensure that fatigue factors have the minimal influence on the experimental results. If the participants feel tired, we will terminate the experiment immediately.

The same performance indicators RMSE and TSR are used to describe the tremor suppression performance. In formula (30), RMSE value is used to quantify the tracking Test 3 (y_i) deviates from the designated tracking Test 1 (r_i) after tremor

suppression based on FES. In formula (31), where $\triangle y$ is the deviation between tracking Test 3 (y_i) and designated tracking Test 1 (r_i). $\triangle v$ is the deviation between tracking Test 2 (v_i) and designated tracking Test 1 (r_i).

The experimental results of Participant No.1 with different control algorithms are shown in Fig. 14. In this experiment, the sample period T_s is 0.005s. The frequencies of tremor signal are set to 2Hz and 2.5Hz. The delay period of the repetitive controller is 100 and 80 respectively. The gains $K_1 = K_2 = 0.5$. The first order low pass filter $Q(z) = 0.25z + 0.5z^0 + 0.25z^{-1}$. The order and cut-off frequency of high-pass Butterworth filter of the PI-HF controller are selected as 6th and 1.2Hz respectively.

From Fig. 14 (a),(b),(c),(d), we can see that Test 1 confirms that participants can voluntarily track the designated reference trajectory task by flexing and extending wrist. Test 2 examined the effect of induced tremor on unimpaired participants to conduct the same tracking task. The experimental results in Test 3 show that FES based wrist tremor suppression with feedback controllers can attenuate the amplitude of tremor without interference with voluntary wrist motion. As shown clearly by experimental results during 13 to 14 seconds in Fig. 14 (e), FMI-MP-RC algorithm and GB-MP-RC algorithm can get substantially better tremor suppression performance than the other two control algorithms.

The quantitative performance index can more intuitively describe the performance of the four control algorithms for FES based tremor suppression. Experimental results of Participant No.1 with different control algorithms and different controller parameters are shown in Table. V.

TABLE V
EXPERIMENTAL RESULTS OF PARTICIPANT NO.1

Controller Type	Controller Parameters	RMSE(°)	TSR
FMI-MP-RC	m = 30,n = 24	1.36	87.65%
	m = 41,n = 36	1.27	89.17%
	m = 52,n = 47	1.17	90.18%
GB-MP-RC	γ = 65	1.42	86.97%
	γ = 85	1.31	88.23%
	γ = 115	1.18	90.11%
FMI-SP-RC	m = 30,n = 24	2.83	73.19%
	m = 41,n = 36	2.41	73.27%
	m = 52,n = 47	2.33	73.93%
PI-HF	K_{P} = 70,K_{I} = 70	3.25	69.58%
	K_{P} = 65,K_{I} = 65	3.12	69.81%
	K_{P} = 60,K_{I} = 60	3.33	68.30%

As seen from Table V, the RMSE values of FMI-MP-RC algorithm and GB-MP-RC algorithm are almost the same, while the other two control algorithms are much greater. The highest TSR of FMI-MP-RC algorithm and GB-MP-RC algorithm are about 90.18% and 90.11% respectively, while the highest TSR values provided by the FMI-SP-RC and PI-HPF algorithms are only 73.94% and 69.81%, which confirm the advantage of multi-periodic repetitive control for multiple frequencies tremor suppression. In summary, the two MP-RC algorithms have the best tremor suppression performance for multi-frequency tremor signals according to Participant No.1.

The experimental results of the other three participants are all similar to those of Participant No.1 and are given

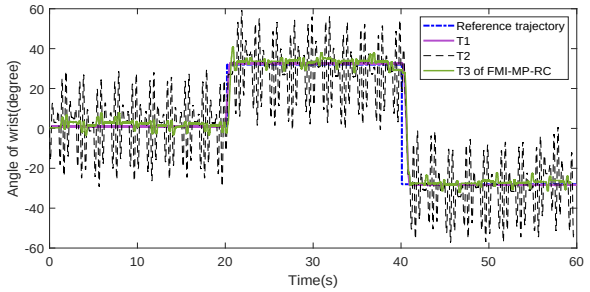

(a)

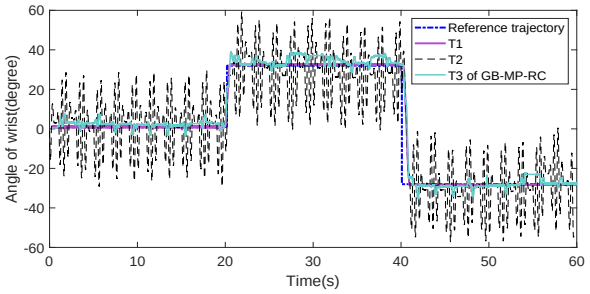

(b)

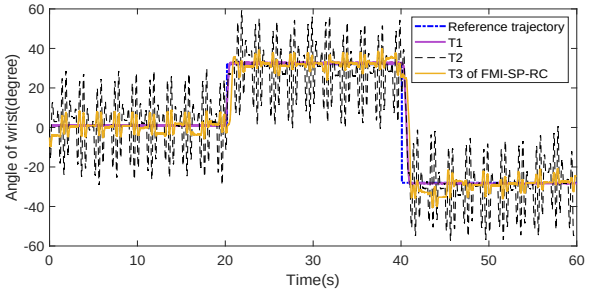

(c)

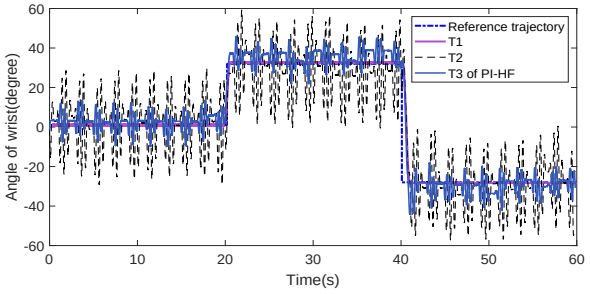

(d)

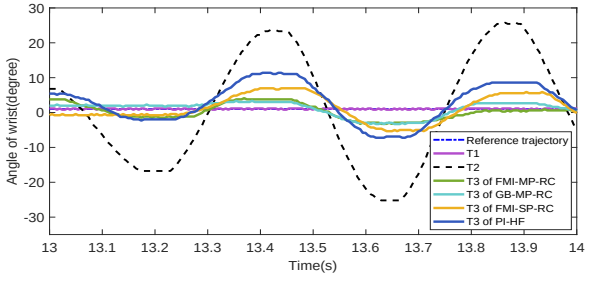

(e)

Fig. 14. (a,b,c,d) Wrist angular position under different controllers of Participant No.1; (e) Wrist angular position under different controllers during 13s to 14s

in Table VI. All the maximum TSR are achieved by the proposed FMI-MP-RC algorithm and GB-MP-RC algorithm. By contrast, the TSR obtained by FMI-SP-RC algorithm and PI-HF control algorithms are greatly lower. The minimum TSR of four participants are all obtained by PI-HF control algorithm. It is also worth mentioning due to the different sensitivity of each person to the electrical stimulation signal, the same control algorithm has different tremor suppression performance in different participants. For example, the average TSR of FMI-MP-RC algorithm of Participant No. 2 is 89.86%, while that of Participant No. 3 is only 83.55%.

TABLE VI
EXPERIMENTAL RESULTS OF OTHER PARTICIPANTS

	Controller Type	Controller Parameters	RMSE(°)	TSR
Participant 2	FMI-MP-RC	m = 45,n = 37	1.25	89.19%
		m = 56,n = 42	1.03	90.52%
	GB-MP-RC	γ = 90	1.31	88.67%
		γ = 120	1.09	90.34%
	FMI-SP-RC	m = 45,n = 37	3.09	71.79%
		m = 56,n = 42	2.92	72.28%
	PI-HF	K_{P} = 60,K_{I} = 60	3.89	64.50%
		K_{P} = 65,K_{I} = 65	3.67	66.64%
Participant 3	FMI-MP-RC	m = 49,n = 46	1.69	82.51%
		m = 59,n = 53	1.67	84.59%
	GB-MP-RC	γ = 95	1.68	82.96%
		γ = 115	1.68	83.27%
	FMI-SP-RC	m = 49,n = 46	3.87	66.18%
		m = 59,n = 53	3.30	69.27%
	PI-HF	K_{P} = 60,K_{I} = 60	4.50	53.29%
		K_{P} = 65,K_{I} = 65	4.16	58.56%
Participant 4	FMI-MP-RC	m = 42,n = 36	1.45	86.65%
		m = 52,n = 46	1.20	89.71%
	GB-MP-RC	γ = 100	1.52	85.17%
		γ = 120	1.30	89.03%
	FMI-SP-RC	m = 42,n = 36	3.49	67.73%
		m = 52,n = 46	3.06	71.84%
	PI-HF	K_{P} = 60,K_{I} = 60	3.62	67.04%
		K_{P} = 65,K_{I} = 65	3.57	67.13%

Statistical analysis results of four participants is given in Table VII. It is illustrated in Table VII that the performance of tremor suppression is substantially enhanced by the proposed multi-periodic repetitive control algorithm: the TSR of the FMI-MP-RC algorithm and GB-MP-RC algorithm are about 23% higher than that of the traditional filter based feedback controller and about 17% higher than that of FIM-SP-RC algorithm on average.

TABLE VII
STATISTICAL ANALYSIS RESULTS OF FOUR PARTICIPANTS

Controller	Phase II*
FMI-MP-RC	87.80% ± 2.74%
GB-MP-RC	87.19% ± 2.79%
FMI-SP-RC	70.05% ± 2.70%
PI-HF	64.98% ± 5.54%

* value: mean ± standard deviation, $n = 9$
n is the number of experiments for each control algorithm.

3) Experimental results-Phase III: After the FES based tremor suppression tests of unimpaired participants, we also carried out experiments on the intention tremor patient (male, 47 years old).

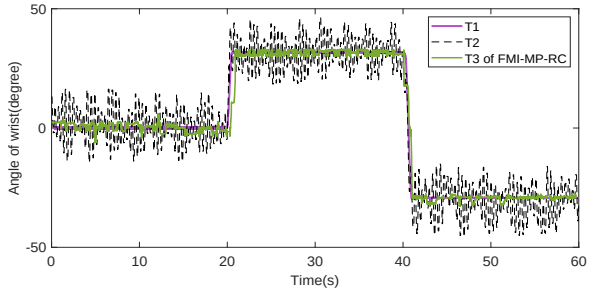

(a)

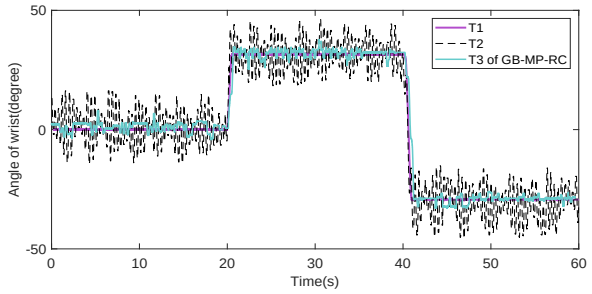

(b)

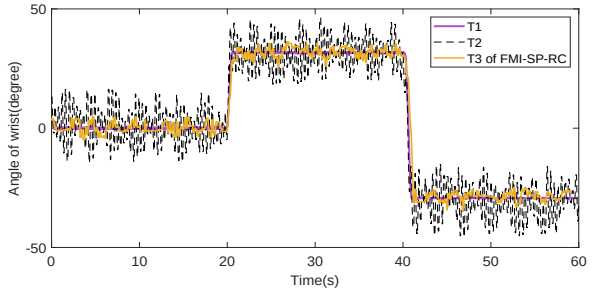

(c)

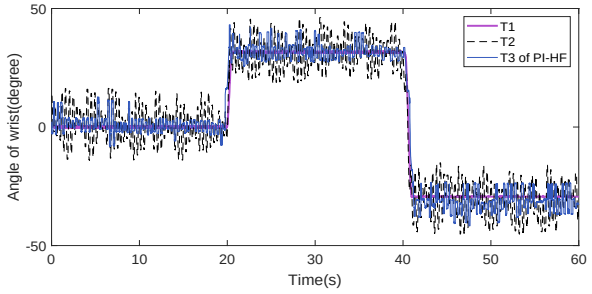

(d)

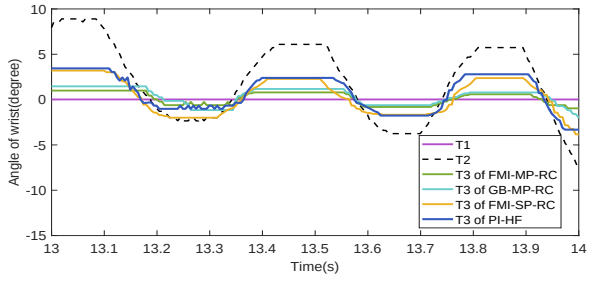

(e)

Fig. 15. (a,b,c,d) Wrist angular position under different controllers of patient; (e) Wrist angular position under different controllers during 13s to 14s

To compare with the results in Phase II, we redefined the following three tests.

Test 1 (T1): The designated reference trajectory is given to the patient (without requiring the patient to do anything).

Test 2 (T2): Track designated trajectory (T1) without FES.

Test 3 (T3): Track designated trajectory (T1) with FES.

The experimental results of the tremor patient are shown in Fig. 15. The main frequencies of the patient are 2.3Hz and 2.5Hz.

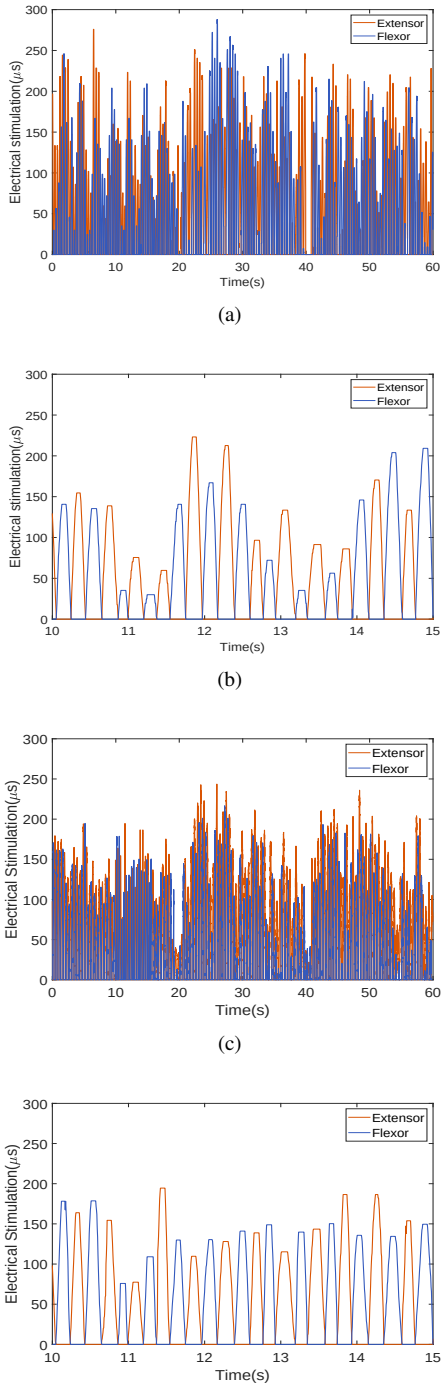

Fig. 16. (a) FES signals generated by FMI-MP-RC controller; (b) FES signals during 10s to 15s (FMI-MP-RC); (c) FES signals generated by GB-MP-RC controller; (d) FES signals during 10s to 15s (GB-MP-RC)

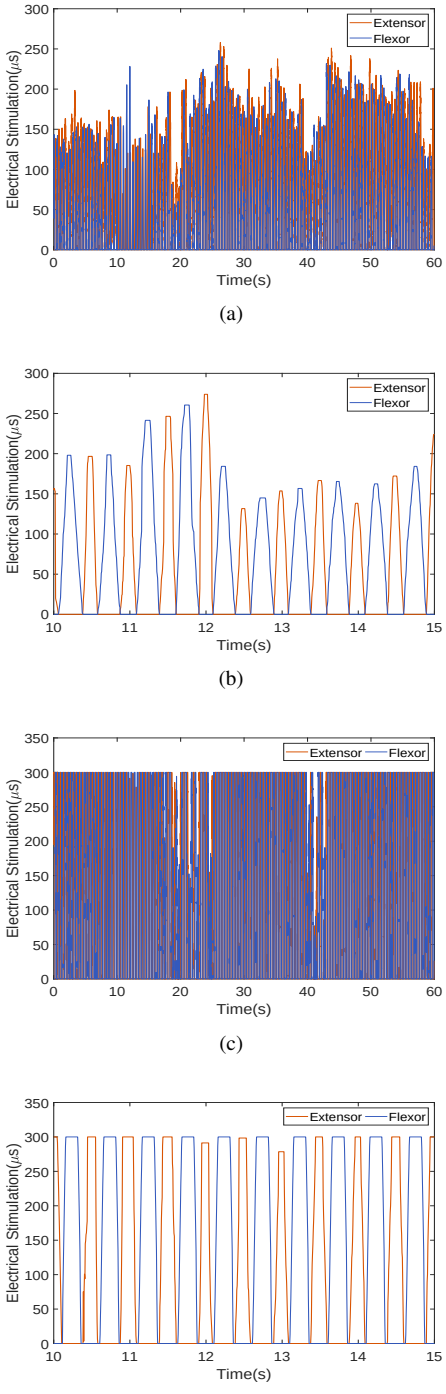

Fig. 17. (a) FES signals generated by FMI-SP-RC controller; (b) FES signals during 10s to 15s (FMI-SP-RC); (c) FES signals generated by PI-HF controller; (d) FES signals during 10s to 15s (PI-HF)

Fig. 15 show that while the tremor amplitudes are all reduced under different FES based controllers, it is clearly seen from Fig. 15 (e), the proposed multi-periodic repetitive control algorithms have better tremor suppression performance than the traditional filter based algorithm and single periodic repetitive control algorithm.

The corresponding FES level generated by the proposed multi-periodic control methods (FMI-MP-RC algorithm and GB-MP-RC algorithm) and the other two control methods

(FMI-SP-RC algorithm and PI-HF algorithm) are shown in Fig. 16 and Fig. 17 respectively. The two channel FES signals are applied to the wrist flexor and extensor through the electrodes to contract the corresponding muscle. At any stage, only one channel is stimulated and this is regulated by the designed feedback controller. When the angle error is positive, the FES signal is applied to wrist extensor, otherwise, FES signal is applied to wrist flexor.

Under each controller, the patient was asked to do the tremor suppression test (T3) four times. The experimental statistical analysis results of the patient is indicated in Table VIII. As shown in Table VIII, the experimental results are consistent with observations in Phase II for unimpaired participants. The FMI-MP-RC and GB-MP-RC can suppress tremor by up to 82.21% and 80.24% respectively on average, while FMI-SP-RC and PI-HF algorithms only achieve average decrease of 67.88% and 52.33% in tremor suppression. The average TSR of the FMI-MP-RC algorithm and GB-MP-RC algorithm are about 14% and 29% higher than FIM-SP-RC algorithm and PI-HF algorithm respectively.

TABLE VIII
STATISTICAL ANALYSIS RESULTS OF PATIENT

Controller Type	Controller Parameters	RMSE(°)†	TSR†
FMI-MP-RC	m = 52,n = 47	0.69 ± 0.09	82.21% ± 1.79%
GB-MP-RC	γ = 115	0.77 ± 0.05	80.24% ± 1.32%
FMI-SP-RC	m = 52,n = 47	1.18 ± 0.04	67.88% ± 1.22%
PI-HF	K_{P} = 65,K_{I} = 65	1.75 ± 0.07	52.33% ± 1.40%

† value: mean ± standard deviation, $n = 4$
n is the number of experiments for each control algorithm.

The tremor suppression performance of four control algorithms for all the experiments are illustrated in Fig. 18. The TSR values of the proposed multi-periodic repetitive control algorithms are substantially higher than the other two control algorithms, which show their superiority and effectiveness.

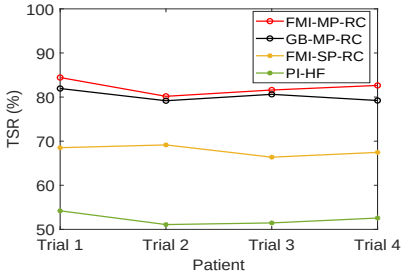

Fig. 18. Tremor suppression rate of tremor patient for each trial

V. CONCLUSION

In this paper, a multi-periodic repetitive controller for FES is proposed to suppress wrist multi frequency tremor. To achieve this, the nonlinear Hammerstein structure is used to model the wrist musculoskeletal system. And then, a controller combining linearization control and feedback repetitive control is proposed. Stability of the proposed design is analyzed and two implementation algorithms are developed. Both simulation and experimental testings are conducted to demonstrate the effectiveness of the proposed design. The experimental results show that substantial improvement in tremor suppression can be achieved by the proposed FMI-MP-RC algorithm and GB-MP-RC algorithm.

While the above results are promising, there are some issues to be further considered. Firstly, the optimisation based repetitive control design will be explored in multi-frequency tremor suppression system to further improve the performance and a lower order multi-periodic RC will be developed to improve computational efficiency. Secondly, tremor frequency is assumed to be fixed in this paper because we used off-line tremor frequency to carry out the experiment. However, the frequency of tremor can vary with time in reality. To address this problem, a possibility is to design multiple-model switched adaptive repetitive controller based on frequency variation which can potentially obtain better performance of tremor suppression and improve the practical application value of the system. Thirdly, there are inevitable model uncertainties associated with the wrist musculoskeletal model used in controller design, a rigorous analysis and further improvement of the robustness performance of the repetitive controller is also a problem to be considered in the future research. Fourthly, in the next stage of our research, muscle fatigue will be incorporated into the design by explicitly including a model of muscle fatigue [43], and/or developing possible ways of reducing the required FES levels. Finally, the experimental results of healthy participants and intention tremor patient confirm the feasibility and effectiveness of this paper. More testing will be undertaken with intention tremor patients and application of the proposed design to other types of tremor patients (e.g. Parkinsons patients) will be investigated to examine whether the proposed approach is capable to produce significant tremor suppression.

APPENDIX I
PROOF OF THE THEOREM 1

The relationship among error $e(k)$, reference $r(k)$ and the disturbance $d(k)$ can be written as

$$e(k) = \frac{1}{1+P(z)C(z)}r(k) - \frac{P(z)}{1+P(z)C(z)}d(k). \quad (32)$$

Substituting (8) into (32), the characteristic polynomial of the closed-loop control system is given below,

$$1 + P(z)H(z)\sum_{p=1}^{n}\frac{Q(z)z^{-N_p}}{1-Q(z)z^{-N_p}}K_p = 0. \quad (33)$$

If the roots of the characteristic polynomial are all within the unit circle, the closed-loop feedback control system is asymptotically stable.

Especially, when $H(z) = P^{-1}(z)$ and $Q(z) = 1$, the p^{th} internal model can be expressed as

$$G_{\mathrm{IM}p}(z) = \frac{1}{z^{N_p}-1}, p = 1, 2, \cdots, n. \quad (34)$$

Let

$$z^{N_p} = r^{N_p}e^{i(N_P\varphi_r)}, \quad (35)$$

where r and φ_r represent the magnitude and phase of z. Then (34) can be rewritten as

$$\begin{aligned} G_{\mathrm{IM}p}(z) &= \frac{1}{r^{N_p}e^{i(N_P\varphi_r)}-1} \\ &= \frac{r^{N_p}\cos(N_p\varphi_r)-1-ir^{N_p}\sin(N_p\varphi_r)}{(r^{N_p}\cos(N_p\varphi_r)-1)^2+(r^{N_p}\sin(N_p\varphi_r))^2}. \end{aligned} \tag{36}$$

The real part of $G_{\mathrm{IM}p}(z)$ is given by

$$Re(G_{\mathrm{IM}p}(z)) = \frac{r^{N_p}\cos(N_p\varphi_r)-1}{r^{2N_p}-2r^{N_p}\cos(N_p\varphi_r)+1}. \tag{37}$$

For any z outside the unit circle ($|z| \geq 1$), i.e. $|r| \geq 1$, we have

$$2(r^{N_p}\cos(N_p\varphi_r)-1) \geq -(r^{2N_p}-2r^{N_p}\cos(N_p\varphi_r)+1), \tag{38}$$

which is equivalent to

$$\frac{r^{N_p}cos(N_p\varphi_r)-1}{r^{2N_p}-2r^{N_p}cos(N_p\varphi_r)+1} \geq -\frac{1}{2}, \tag{39}$$

and thus

$$Re(G_{\mathrm{IM}p}(z)) \geq -\frac{1}{2}, \forall |z| \geq 1. \tag{40}$$

From the above relationship, we can show

$$Re(\sum_{p=1}^{n} G_{\mathrm{IM}p}(z)K_p) \geq -\frac{1}{2}\sum_{p=1}^{n} K_p, \forall |z| \geq 1. \tag{41}$$

Therefore, if condition (12) is satisfied, i.e. $\sum_{p=1}^{n} K_p < 2$, $K_p > 0$, $(p = 1, 2, ...n)$, the real part of characteristic polynomial (11) is

$$Re(1+\sum_{p=1}^{n} G_{\mathrm{IM}p}K_p) = 1 + Re(\sum_{p=1}^{n} G_{\mathrm{IM}p}K_p) > 0, \forall |z| \geq 1, \tag{42}$$

i.e. the characteristic polynomial

$$1+\sum_{p=1}^{n} G_{\mathrm{IM}p}K_p \neq 0, \forall |z| \geq 1. \tag{43}$$

Therefore, if condition (12) is satisfied, all the roots of the characteristic polynomial are within the unit circle.

That completes the proof. ■

REFERENCES

[1] J. K. McCreary, J. A. Rogers, and S. J. Forwell. Upper limb intention tremor in multiple sclerosis: an evidence-based review of assessment and treatment. *International Journal of MS Care*, 20(5):211–223, 2018.

[2] R. J. Elble. Tremor. In *Neuro-Geriatrics*, pages 311–326. Springer, 2017.

[3] E. J. Smits, A. J. Tolonen, L. Cluitmans, M. V. Gils, et al. Graphical tasks to measure upper limb function in patients with parkinson's disease: Validity and response to dopaminergic medication. *IEEE Journal of Biomedical & Health Informatics*, 21(1):283–289, 2017.

[4] S. S. Raju, A. Niranjan, E. A. Monaco, J. C. Flickinger, and L. D. Lunsford. Stereotactic radiosurgery for medically refractory multiple sclerosis–related tremor. *Journal of Neurosurgery*, 128(4):1214–1221, 2018.

[5] L. Cif and M. Hariz. Seventy years of pallidotomy for movement disorders. *Movement Disorders*, 32(7):972–982, 2017.

[6] K. P. Michmizos, B. Lindqvist, S. Wong, E. L. Hargreaves, K. Psychas, G. D. Mitsis, S. F. Danish, and K. S. Nikita. Computational neuromodulation: Future challenges for deep brain stimulation. *IEEE Signal Processing Magazine*, 34(2):114–119, 2017.

[7] S. F. Paul, W. J. Elias, P. Ghanouni, et al. Neurological adverse event profile of magnetic resonance imaging–guided focused ultrasound thalamotomy for essential tremor. *Movement Disorders*, 33(5):843–847, 2018.

[8] E. Rocon, J. Gallego, J. M. Belda-Lois, et al. Biomechanical loading as an alternative treatment for tremor: a review of two approaches. *Tremor and other hyperkinetic movements*, 2:601–603, 2012.

[9] Q. Zhang, M. Hayashibe, and C. Azevedo-Coste. Evoked electromyography-based closed-loop torque control in functional electrical stimulation. *IEEE Transactions on Biomedical Engineering*, 60(8):2299–2307, 2013.

[10] E. J. Gonzalez, R. J. Downey, C. A. Rouse, and W. E. Dixon. Influence of elbow flexion and stimulation site on neuromuscular electrical stimulation of the biceps brachii. *IEEE Trans Neural System Rehabilitation Enginering*, 26(4):904–910, 2018.

[11] C. T. Freeman, K. Yang, J. Tudor, and M. Kutlu. Feedback control of electrical stimulation electrode arrays. *Medical Engineering & Physics*, 38(11):1185–1194, 2016.

[12] M. Javidan, J. Elek, and A. Prochazka. Attenuation of pathological tremors by functional electrical stimulation II: clinical evaluation. *Annals of Biomedical Engineering*, 20(2):225–236, 1992.

[13] A. P. L. Bó, L. O. da Fonseca, and A. C. C. de Sousa. FES-induced coactivation of antagonist muscles for upper limb control and disturbance rejection. *Medical Engineering & Physics*, 38(11):1176–1184, 2016.

[14] D. Zhang, P. Poignet, F. Widjaja, and T. A. Wei. Neural oscillator based control for pathological tremor suppression via functional electrical stimulation. *Control Engineering Practice*, 19(1):74–88, 2011.

[15] E. H. Copur, C. T. Freeman, B. Chu, and D. S. Laila. Repetitive control of electrical stimulation for tremor suppression. *IEEE Transactions on Control Systems Technology*, 27(2):540–552, 2019.

[16] P. H. Peckham and J. S. Knutson. Functional electrical stimulation for neuromuscular applications. *Annual Review of Biomedical Engineering*, 7:327–360, 2005.

[17] A. Prochazka, J. Elek, and M. Javidan. Attenuation of pathological tremors by functional electrical stimulation I: Method. *Annals of Biomedical Engineering*, 20(2):205–224, 1992.

[18] D. M. Gillard, T. Cameron, A. Prochazka, and M. J. Gauthier. Tremor suppression using functional electrical stimulation: a comparison between digital and analog controllers. *IEEE transactions on Rehabilitation Engineering*, 7(3):385–388, 1999.

[19] D. Zhang and W. T. Ang. Tremor suppression of elbow joint via functional electrical stimulation: A simulation study. In *2006 IEEE International Conference on Automation Science and Engineering*, pages 182–187. IEEE, 2006.

[20] R. J. Verstappen, C. T. Freeman, E. Rogers, et al. Robust higher order repetitive control applied to human tremor suppression. In *2012 IEEE International Symposium on Intelligent Control*, pages 1214–1219. IEEE, 2012.

[21] C. T. Freeman, P. Sampsonb, J. H. Burridgeb, and A. M. Hughesb. Repetitive control of functional electrical stimulation for induced tremor suppression. *Mechatroics*, 32:79–87, 2015.

[22] Y. Zhou, M. E. Jenkins, M. D. Naish, and A. L. Trejos. Characterization of parkinsonian hand tremor and validation of a high-order tremor estimator. *IEEE Transactions on Neural Systems and Rehabilitation Engineering*, 26(9):1823–1834, 2018.

[23] A. Kovács, M. Kiss, N. Pintér, I. Szirmai, and A. Kamondi. Characteristics of tremor induced by lesions of the cerebellum. *The Cerebellum*, 18(4):705–720, 2019.

[24] Z. Zhang, B. Chu, Y. Liu, and D. H. Ownens. FES based wrist tremor suppression using multi-periodic repetitive control. *21st IFAC World Congress*, 2020.

[25] K. P. Bhatia, P. Bain, N. Bajaj, et al. Consensus statement on the classification of tremors. From the task force on tremor of the international parkinson and movement disorder society. *Movement Disorders*, 33(1):75–87, 2018.

[26] J. Ding, A.S. Wexler, and S.A. Binder-Macleod. A predictive model of fatigue in human skeletal muscles. *Journal of Applied Physiology*, 89(4):1322–1332, 2000.

[27] J. Ding, A.S. Wexler, and S.A. Binder-Macleod. A mathematical model that predicts the force–frequency relationship of human skeletal muscle. *Muscle & Nerve: Official Journal of the American Association of Electrodiagnostic Medicine*, 26(4):477–485, 2002.

[28] F. Le, I. Markovsky, C.T. Freeman, and E. Rogers. Recursive identification of hammerstein systems with application to electrically stimulated muscle. *Control Engineering Practice*, 20(4):386–396, 2012.

[29] K. J. Hunt, M. Munih, N.N. Donaldson, and F.M. Barr. Investigation of the hammerstein hypothesis in the modeling of electrically stimulated muscle. *IEEE Transactions on Biomedical Engineering*, 45(8):998–1009, 1998.

[30] G. M. Lyons, G. E. Leane, M. M. Clarke, J. V. O'brien, and P. A. Grace. An investigation of the effect of electrode size and electrode location on comfort during stimulation of the gastrocnemius muscle. *Medical Engineering & Physics*, 26(10):873–878, 2004.

[31] F. M. Colacino, R. Emiliano, and B. R. Mace. Subject-specific musculoskeletal parameters of wrist flexors and extensors estimated by an emg-driven musculoskeletal model. *Medical Engineering & Physics*, 34(5):531–540, 2012.

[32] M. Curtin and M. M. Lowery. Musculoskeletal modelling of muscle activation and applied external forces for the correction of scoliosis. *Journal of Neuroengineering and Rehabilitation*, 11(1):52, 2014.

[33] S. Takehara, M. Murakami, and K. Hase. Biomechanical evaluation of an electric power-assisted bicycle by a musculoskeletal model. *Journal of System Design and Dynamics*, 6(3):343–350, 2012.

[34] J. A. Gallego, J. L. Dideriksen, A. Holobar, J. Ibáñez, V. Glaser, J. P. Romero, J. Benito-León, J. Pons, E. Rocon, and D. Farina. The phase difference between neural drives to antagonist muscles in essential tremor is associated with the relative strength of supraspinal and afferent input. *Journal of Neuroscience*, 35(23):8925–8937, 2015.

[35] J. Raethjen, M. Lindemann, H. Schmaljohann, R. Wenzelburger, G. Pfister, and G. Deuschl. Multiple oscillators are causing parkinsonian and essential tremor. *Movement Disorders: Official Journal of the Movement Disorder Society*, 15(1):84–94, 2000.

[36] W. S. Chang, I. H. Suh, and J. H. Oh. Synthesis and analysis of digital multiple repetitive control systems. In *American Control Conference*, pages 2687–2691, 1998.

[37] M. Steinbuch, Siep W., and Tarunraj S. Design of noise and period-time robust high-order repetitive control, with application to optical storage. *Automatica*, 43(12):2086–2095, 2007.

[38] R. W. Longman. On the theory and design of linear repetitive control systemsg. *European Journal of Control*, 16(5):447–496, 2010.

[39] J. J. Hätönen, C.T. Freeman, D.H. Owens, P. L. Lewin, and E. Rogers. A gradient-based repetitive control algorithm combining ILC and pole placement. *European Journal of Control*, 12(3):278–292, 2006.

[40] W. K. Durfee and K. E. MACLean. Methods for estimating isometric recruitment curves of electrically stimulated muscle. *IEEE Transactions on Biomedical Engineering*, 36(7):654–667, 1989.

[41] T. A. Saifee. Tremor. *British Medical Bulletin*, 130:51–63, 2019.

[42] C. L. Lynch and Milos . R. Popovic. Functional electrical stimulation. *IEEE Control Systems Magazine*, 28(2):40–50, 2008.

[43] F . Luijten, B . Chu, and E. Rogers. Iterative learning control for stroke rehabilitation with input dependent muscle fatigue modeling. In *2018 Annual American Control Conference (ACC)*, pages 6396–6401. IEEE, 2018.